Physics Letters B 732 (2014) 228–232

Contents lists available at ScienceDirect

Physics Letters B

www.elsevier.com/locate/physletb

Four-body effects in the ^{6}He + ^{58}Ni scattering

V. Morcelle [a,b], K.C.C. Pires [c,d], M. Rodríguez-Gallardo [e], R. Lichtenthäler [d,*], A. Lépine-Szily [d], V. Guimarães [d], P.N. de Faria [b], D.R. Mendes Junior [b], A.M. Moro [e], L.R. Gasques [d], E. Leistenschneider [d], R. Pampa Condori [d], V. Scarduelli [d], M.C. Morais [f], A. Barioni [g], J.C. Zamora [i], J.M.B. Shorto [h]

[a] Universidade Federal de Itajubá, Campus Itabira, MG 35900-030, Brazil
[b] Instituto de Física, Universidade Federal Fluminense, Niterói, RJ 24210-340, Brazil
[c] Universidade Tecnológica Federal do Paraná, Campus Cornélio Procópio, PR 86300-000, Brazil
[d] Instituto de Física, Universidade de São Paulo, C.P. 66318, 05389-970 São Paulo, Brazil
[e] Departamento de FAMN, Facultad de Física, Universidad de Sevilla, Apdo. 1065, E-41080 Sevilla, Spain
[f] Centro Brasileiro de Pesquisas Físicas, CBPF, Rio de Janeiro, RJ 22290-180, Brazil
[g] Departamento de Física da Terra e do Meio Ambiente, Instituto de Física, Universidade Federal da Bahia, Campus Ondina, BA 40210-340, Brazil
[h] Instituto de Pesquisas Energeticas e Nucleares – IPEN, 05508-000 São Paulo, Brazil
[i] Technische Universität Darmstadt, Germany

ARTICLE INFO

Article history:
Received 19 December 2013
Received in revised form 12 March 2014
Accepted 19 March 2014
Available online 26 March 2014
Editor: V. Metag

ABSTRACT

We present angular distributions of the ^{6}He + ^{58}Ni scattering measured at three bombarding energies above the Coulomb barrier: $E_{\rm lab} = 12.2$ MeV, 16.5 MeV, and 21.7 MeV. The angular distributions have been analysed in terms of three- and four-body Continuum-Discretized Coupled-Channels calculations considering the effect of the ^{6}He breakup. A behaviour in the cross section at large angles has been observed which was reproduced only by the four-body Continuum-Discretized Coupled-Channels calculation.

1. Introduction

Low-energy reactions induced by light exotic nuclei have been investigated over the last years using secondary beams of ^{6}He, ^{11}Be, and ^{11}Li [1–7]. These nuclei show a common characteristic which is their cluster structure, composed by a 'stable' core plus one or two weakly bound neutrons. Due to the low binding energies and low angular momenta of the valence neutrons, their wave function extends over large distances from the core, forming a kind of halo whose density is much lower than the normal nuclear matter. In addition, ^{6}He and ^{11}Li are examples of three-body systems in nature. They are called Borromean nuclei (in allusion to the Borromean rings) and are bound only if their three constituents are present. The ^{6}He nucleus is composed by an alpha particle plus two neutrons, but any binary sub-system of its components is unbound, ^{5}He is unbound and so is the di-neutron system.

The characteristics of such light neutron rich nuclei make them very interesting in several aspects. Some of them may play a role in astrophysical explosive scenarios [8–11], acting as bridges to overcome the instability gaps at $A = 5$ and $A = 8$ and participating in the synthesis of heavier elements. They may also have importance in more general issues such as in the many-body problem in physics and the possible existence of three-body states such as Efimov resonances [12,13].

The fact that some exotic nuclei present a neutron halo has consequences from the reaction mechanism and the nuclear structure points of view. Due to their low binding energies, 0.973 MeV for ^{6}He, 0.5 MeV for ^{11}Be, and 0.37 MeV for ^{11}Li, these projectiles are likely to breakup in the collision with a target. Moreover, the long range of the neutron halo increases its reactivity favouring one and two neutron transfer reactions [14]. Due to the loosely-bound neutrons, reactions can occur even at energies around and below the Coulomb barrier and can take place at rather large distances from the target.

From the experimental point of view, some characteristics have been observed in the elastic scattering of exotic beams which differ from collisions with stable projectiles. The elastic angular distributions of ^{6}He and ^{11}Li on heavy targets such as ^{120}Sn [2] and ^{208}Pb [15,6,7], and ^{11}Be on intermediate mass targets such as ^{64}Zn [4], present a damping of the Fresnel oscillations which is usually observed at forward scattering angles and at energies above the Coulomb barrier. On the other hand, a considerable enhancement in the total reaction cross section with respect to the stable nuclei

* Corresponding author.

http://dx.doi.org/10.1016/j.physletb.2014.03.043

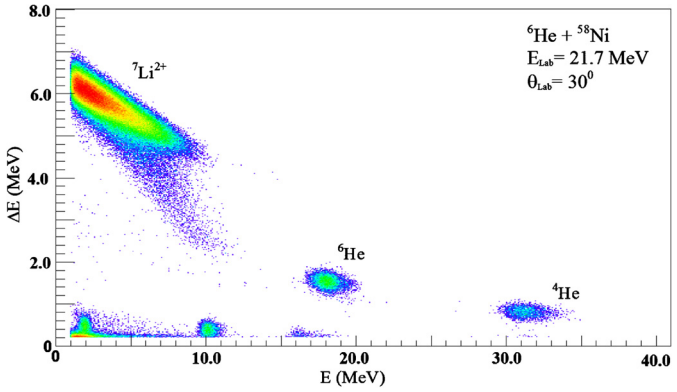

Fig. 1. (Color online.) Two-dimensional spectrum obtained with the ^{6}He beam and ^{58}Ni target at $\theta_{\rm lab} = 30^{\circ}$ and $E_{\rm lab} = 21.7$ MeV.

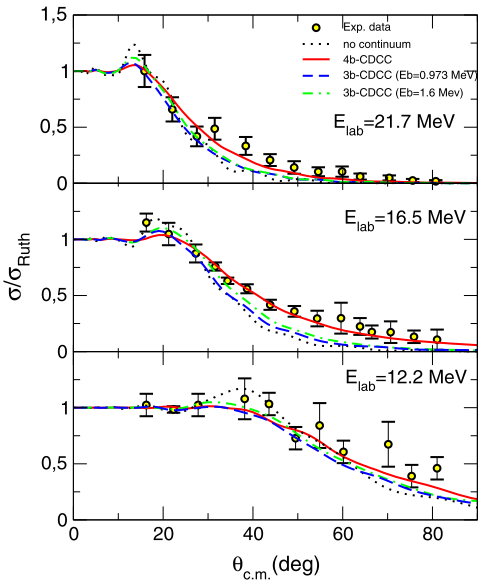

Fig. 2. (Color online.) Elastic angular distributions for ^{6}He + ^{58}Ni system at $E_{\rm lab} = 21.7$ MeV (upper panel), 16.5 MeV (middle panel), and 12.2 MeV (lower panel). Three- and four-body CDCC calculations are also shown.

with similar masses has been observed [2,5]. Both phenomena are related to each other and have been interpreted as a consequence of the coupling with the projectile breakup and possibly the neutron transfer reactions. In first order, the breakup removes flux from the elastic scattering and takes place either in the long-range Coulomb field (Coulomb breakup) or in the short-range nuclear field (nuclear breakup) [16]. Coulomb breakup dominates at large distances, where the nuclear short-range interaction is negligible and the high angular-momentum partial waves participate, thus removing flux at corresponding forward angles. A similar phenomenon has been seen in the past (see for instance [17]) for heavy stable systems in which the Coulomb excitation is an important reaction channel. As we go to lighter targets the Coulomb interaction becomes less important and for very light systems the nuclear breakup dominates. Nuclear breakup is a diffractive process which takes place in a localized space region around the surface of the colliding nuclei where the short-range nuclear interaction is dominant. As a consequence, it tends to affect more the large angles region as it was seen in the ^{6}He + ^{9}Be scattering [3], where the breakup effects appear mainly at large angles. Here we present new data for ^{6}He on an intermediate mass target, ^{58}Ni.

2. Experimental setup

The experiment was performed in the São Paulo Pelletron Accelerator using the RIBRAS system [18,19]. A ^{7}Li^{3+} primary beam of energies $E_{\rm lab} = 18.0, 22.0,$ and 27.0 MeV and intensity of $I \approx$ 200 nAe was used to produce the ^{6}He^{2+} secondary beam by the ^{9}Be(^{7}Li,^{6}He)^{10}B reaction in the primary target of RIBRAS. The primary beam intensity was measured by a Faraday cup (which covers $0 \leqslant \theta \leqslant 2$ degrees) connected to a current integrator to provide the total incident charge at each run. A 12 μm ^{9}Be foil was used as primary target. The secondary target consisted of a ^{58}Ni isotopically enriched foil of 2.2 mg/cm^{2}. The selection of the secondary beam was performed by the first solenoid of the RIBRAS system. Four E (1000 μm)–ΔE (20 μm) telescopes formed by silicon detectors were mounted in the intermediate scattering chamber to detect and identify the reaction products. A two-dimensional (ΔE–E) spectrum can be seen in Fig. 1.

The secondary beam contaminations at this position can be seen in Fig. 1 as the low-energy peak of ^{7}Li^{2+}, the higher energy peak of α-particles ($E(\alpha) = 1.5E(^{6}\text{He})$) and lighter particles such as deuterons and tritons. These contaminations do not affect our results since they are well separated from the elastic peak. Runs using a ^{197}Au target have been performed during the experiment in order to normalize the data and to monitor the secondary beam intensity. The cross sections have been obtained by normalization with respect to the Gold target runs, for which the cross sections are described solely by Rutherford scattering formula. Thus we obtained expressions for the cross sections which are independent of the solid angles of the detectors [2,3]:

$$\sigma^{^{6}\text{He}+^{58}\text{Ni}}(\theta) = \frac{N_c^{\rm Ni}}{N_c^{\rm Au}} \frac{N_b^{\rm Au}}{N_b^{\rm Ni}} \frac{N_t^{\rm Au}}{N_t^{\rm Ni}} \frac{J^{\rm Ni}}{J^{\rm Au}} \sigma_{Ruth}^{^{6}\text{He}+^{197}\text{Au}}(\theta), \tag{1}$$

where N_c is the area of the peak of interest, N_b is the total number of incident ^{6}He beam particles during the run, N_t is the areal density of the target in atoms/cm^{2} and J is the transformation factor from the laboratory to the center of mass system. The total number of ^{6}He beam particles N_b is proportional to the number of particles of the primary beam $N_b = \varepsilon \times N_{7Li}$, where $\varepsilon \approx 10^{-7}$ is the production rate and N_{7Li} is proportional to I, the primary beam integrator. Then, the equality $\frac{N_b^{\rm Au}}{N_b^{\rm Ni}} = \frac{I^{\rm Au}}{I^{\rm Ni}}$ holds if the production rate ε is constant between different runs.

The ^{6}He + ^{58}Ni angular distributions have been obtained in the $\theta_{\rm lab} = 15^{\circ}$–$75^{\circ}$ angular range with steps of 3° in the laboratory system. They are presented in Fig. 2 for three energies, $E_{\rm lab} = 12.2, 16.5,$ and 21.7 MeV. The error bars of the experimental points are pure statistical and no systematic errors have been included. Statistical errors appear in both terms $N_c^{\rm Ni,Au}$ and have been propagated through the expression above. Possible sources of systematic errors would be in the target thickness ratio and in the ratio of the integrators. The target thicknesses should not give an important contribution to the errors since they have been measured, by energy loss measurements using an alpha-source of ^{241}Am, with a precision of about 7%, which is much smaller than the statistical errors. In addition, systematic deviations in the target thickness measurement would affect the three distributions in the same way.

The ratio of the integrators $I^{\rm Au}/I^{\rm Ni}$ on the other hand could be an additional source of errors due to possible variations in the production rate between Gold and Ni target runs. Variations of about 20% or even more in the production rate have been observed during the experiments. To better control this possible source of errors we performed measurements of the production rate, with Gold target, just before and just after each Ni target run, and used the

Table 1
Optical potentials used in the CDCC calculations at the three energies, respectively, for $\alpha + {}^{58}$Ni (top row) and $n + {}^{58}$Ni (bottom row).

E_{lab} (MeV)	V_0 (MeV)	r_0 (fm)	a_0 (fm)	W_0 (MeV)	r_i (fm)	a_i (fm)	W_d (MeV)	r_d (fm)	a_d (fm)	Ref.
12.2	60.00	1.62	0.54	0.50	1.62	0.54	15.84	1.52	0.44	[31]
	61.36	1.45	0.57	–	–	–	1.28	1.45	0.50	[30]
16.5	165.90	1.62	0.40	11.40	1.62	0.4	23.98	1.52	0.44	[29]
	42.00	1.46	0.35	6.09	1.46	0.35	–	–	–	[29]
21.7	135.10	1.35	0.64	7.64	1.34	0.50	18.97	1.52	0.44	[29]
	42.00	1.46	0.35	6.09	1.46	0.35	–	–	–	[29]

average value of N_b^{Au} and I^{Au} for normalization. We believe that this procedure should account for most of the variations in the production rate.

Additional systematic deviations in the integrator measurements (I^{Au}) could still be present but should be minimized by the procedure of taking the ratios of these quantities, in formula (1). Finally, it is not easy to give a precise determination of the magnitude of remnant systematic errors. Comparisons between data and calculations in previous experiments [2,3] indicate that, differences between 15–20% in the normalization of individual angular distributions could exist. However, in the present experiment, we believe that the errors in the overall normalization of the angular distributions are considerably smaller than that.

3. Analysis of the elastic angular distributions

Theoretical approaches have been developed over the last decades to describe the scattering of neutron (and also proton) halo exotic nuclei [6,20–26]. Due to the low binding energy of the projectiles, there is a strong coupling between the elastic scattering and breakup channels that must be taken into account. The Continuum-Discretized Coupled-Channels (CDCC) [27] framework allows to assess these effects. The CDCC model space includes both, the bound and unbound states of the projectile, allowing the evaluation of the projectile breakup and its consequences on the elastic scattering. Since the unbound states form a continuum of energy and their wave-functions are non-normalizable, in the CDCC formalism the continuum is discretized in terms of energy sub-intervals (bins) up to a maximum energy. A bin is a square-integrable state constructed as a linear superposition of the scattering states in that energy sub-interval.

The CDCC framework was first developed for three-body reactions, i.e., for two-body projectiles such as ^{11}Be. Nevertheless, the three-body CDCC method can be applied to Borromean nuclei such as ^{6}He within a di-neutron model, that is, by assuming a two-body model for ^{6}He consisting of an alpha core plus a di-neutron particle. An improvement in this three-body model was proposed by Moro et al. [28] to take into account four-body effects by using an effective two-neutron separation energy in ^{6}He ($S_{2n} = 1.6$ MeV instead of 0.973 MeV). This modification better reproduces the ^{6}He nucleus ground-state wave function and the $B(E1)$ strength obtained within a three-body model description of ^{6}He. More recently, the CDCC framework has been extended to four-body reactions [24]. Within the four-body CDCC method, the ^{6}He nucleus is described as a three-body system, an alpha core plus two neutrons.

In a previous work [2], the scattering of ^{6}He nucleus on a heavier target, ^{120}Sn, was studied using both, the four- and improved three-body CDCC models. The calculations were very close to each other and reproduced fairly well the experimental elastic data. On the other hand, the same study on a light target, ^{9}Be [3], reveals that the agreement between both models is not that good, mainly at large angles.

In this work, we address the scattering of ^{6}He on a medium-mass target, ^{58}Ni. We perform, and compare with elastic data, standard three-body, improved three-body, and four-body CDCC calculations. The $\alpha + {}^{58}$Ni and $n + {}^{58}$Ni optical potentials used here have been obtained from actual data and are shown in Table 1. The $2n + {}^{58}$Ni potential, used on the standard and improved three-body CDCC calculations, was obtained by a single folding model using the $n + {}^{58}$Ni optical potential, shown in Table 1, and the neutron–neutron density distribution obtained from Ref. [28]. Continuum states with $\ell = 0-4$ were included in the three-body calculation in order to obtain a full convergence. In the present three-body calculations, for each partial wave, the continuum is truncated at a maximum excitation energy of $\varepsilon = 6, 9,$ and 15 MeV respectively for 12.2, 16.5, and 21.7 MeV incident energies, and discretized into about 5 bins, evenly spaced in the linear momentum space. The four-body calculations include bins up to 7, 8, and 9 MeV for the incident energies 12.2, 16.5, and 21.7 MeV, respectively, in order to get convergence. The inclusion of states with angular momenta $J^p = 0^+, 1^-, 2^+, 3^-$ was sufficient. For both, three- and four-body calculations, full convergence is checked by two criteria: the total cross section as a function of the total angular momentum J must converge (be very small) for high J and the elastic angular distributions are not sensitive to variations in the number of bins, the maximum energy, and number of angular momenta used in the calculation [24,28].

The results of the calculations are shown in Fig. 2. The dotted black line is the four-body CDCC without coupling to the continuum. The solid red line corresponds to the full four-body CDCC calculation. The dashed blue and dash-dotted green lines are the three-body calculations with 0.973 MeV and 1.6 MeV two-neutron separation energies, respectively. We can see from Fig. 2 that the effect of the coupling to the breakup channel is clearly the flux removal from the forward angles region, reducing the elastic cross section in the region of the Fresnel peak. This behaviour is well reproduced by the three- and four- body models used here. At large angles, however, we observe that the fall of the angular distribution is less steep than expected by the three-body calculations and it is reproduced only by the four-body calculation. Both three-body calculations fail to reproduce the data in this angular region. The improved three-body model comes closer to the data than the standard three-body, but it is not sufficient to reproduce them.

The results of the CDCC calculations presented here are quite stable with respect to variations in the parameters of the optical potentials of $n + {}^{58}$Ni and $\alpha + {}^{58}$Ni, which, together with the ^{6}He wave function, are the main ingredients to obtain the ^{6}He + ^{58}Ni interaction. We performed variations ($\pm 10\%$) in the strengths V and W, the radius and diffuseness of the 16.5 MeV $n + {}^{58}$Ni optical potential around the values of Table 1 and, the effect in the final three- and four-body calculations was of only a few percent, much smaller than the actual difference between three- and four-body results of Fig. 2. The sensitivity to variations in the $\alpha + {}^{58}$Ni potential was found to be even smaller, as expected since the energies are close to the Coulomb barrier. The sensitivity to variations in the

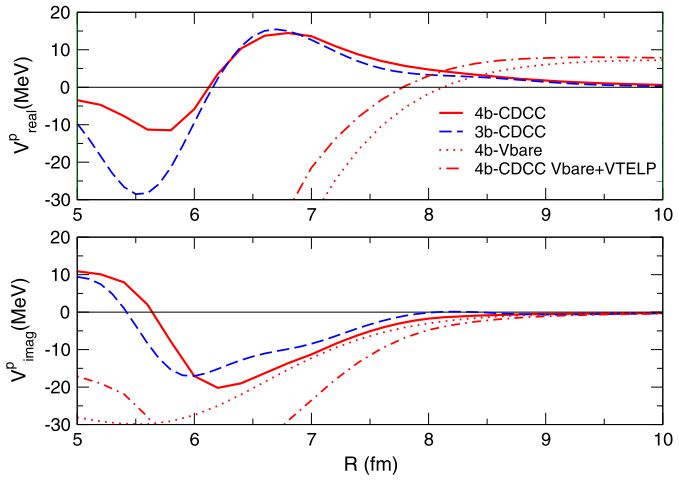

Fig. 3. (Color online.) TELP and Bare potentials from standard three- and four-body CDCC calculations for the ^{6}He + ^{58}Ni system at an incident energy of E_{lab} = 16.5 MeV.

number of bins and of angular momenta used in the calculations was also very small, provided that convergence has been reached.

In order to better understand the dynamics of the coupling to the breakup channel, it is interesting to look at the characteristics of the polarization potential which comes out from the CDCC calculations. Polarization potentials are in general very complicated non-local quantities but, a trivially local equivalent potential (TELP) can be obtained [32] which displays the main features of the coupling. In Fig. 3 we present, for the incident energy E_{lab} = 16.5 MeV, the TELP potential extracted from the CDCC calculations as a function of the distance R between ^{6}He and ^{58}Ni. The polarization potential from the standard three-body CDCC is shown by the dashed blue line and the four-body by a solid red line. We also plot the 4b-Bare (red dotted) and the sum 4b-Bare+TELP (red dash-dot-dash). One of the main characteristics of the polarization potential from breakup is the long-range absorptive imaginary part in the surface region and outwards. This long-range absorption describes the loss of flux to the combined effect of the nuclear and Coulomb breakup. The real part of the polarization potential, on the other side, is repulsive in the region of the surface of the system ($R \approx$ 6–7 fm) and it is due to the nuclear breakup. As we see from the total Bare+TELP curves, the effect of the polarization potential is to enhance the Coulomb barrier, reducing the fusion cross section at this energy.

Similar qualitative characteristics, such as the long range imaginary and the repulsive real potentials, have been observed in the CDCC polarization potentials in lighter systems [3] and seem to be general features of the polarization potentials derived from CDCC calculations, in the case of neutron halo projectiles.

Even in the context of the Optical Model, applied to the analysis of exotic heavy systems such as ^{6}He + ^{120}Sn [33] and others [34], the inclusion of a surface absorptive term in the optical potential appears to be a necessary condition to correctly reproduce the energy dependence of the angular distributions. Such an absorptive surface term simulates the dynamics of peripheral reactions, such as breakup and neutron transfers, that are taking place in the region near to the Coulomb barrier.

Another important information that one can obtain from the elastic scattering is the total reaction cross section. The total reaction cross sections obtained from the present four-body CDCC calculations are of 1185, 1833, and 2185 mb, respectively for E_{lab} = 12.2, 16.5, and 21.7 MeV. We transformed these cross sections and energies using the recipe of Gomes et al. [35], to be able to compare them with data for stable weakly bound systems such as ^{6,7}Li and ^{9}Be [36,37] on similar mass targets. We found a consistent enhancement of about 40–50% in the total reaction cross section for ^{6}He+^{58}Ni with respect to the stable weakly bound ^{6,7}Li and ^{9}Be. This result is in agreement with previous results from similar analysis of intermediate mass and heavy systems [14,39,40]. However, for lighter systems such as ^{6}He + ^{9}Be and ^{6}He + ^{12}C the enhancements are lower, around 25% [38] or less [20].

4. Summary and conclusions

We measured the ^{6}He + ^{58}Ni scattering at three energies slightly above the Coulomb barrier. We performed standard and improved three-body CDCC calculations and the more appropriate four-body CDCC calculations. Both three-body models fail to reproduce the experimental elastic data for the whole angle range. On the other hand, four-body CDCC calculations reproduce very well the experimental data without any parameter adjustment.

Acknowledgements

This work has been partially supported by Conselho Nacional de Desenvolvimento Científico e Tecnológico – CNPq/MCTI (Brazil), proc. No. 303112/2010-7, Fundação de Amparo à Pesquisa do Estado de São Paulo – FAPESP (Brazil), proc. No. 2011/08781-6, Spanish National Project No. FPA2009-07653 and by the Consolider-Ingenio 2010 Program CPAN (CSD2007-00042). M.R.G. acknowledges the finantial support from the program VPPI-US.

References

[1] E.A. Benjamim, et al., Phys. Lett. B 647 (2007) 30.
[2] P.N. de Faria, et al., Phys. Rev. C 81 (2010) 044605.
[3] K.C.C. Pires, et al., Phys. Rev. C 83 (2011) 064603.
[4] A. di Pietro, et al., Phys. Rev. Lett. 105 (2010) 022701.
[5] E.F. Aguilera, et al., Phys. Rev. C 79 (2009) 021601(R).
[6] M. Cubero, et al., Phys. Rev. Lett. 109 (2012) 262701.
[7] J.P. Fernández-García, et al., Phys. Rev. Lett. 110 (2013) 142701.
[8] V. Efros, W. Balogh, H. Herndl, R. Hofinger, H. Oberhummer, Z. Phys. A 335 (1996) 101.
[9] J. Görres, H. Herndl, I.J. Thompson, M. Wiesher, Phys. Rev. C 52 (1995) 2231.
[10] R. de Diego, E. Garrido, D.V. Fedorov, A.S. Jensen, Eur. Phys. Lett. 90 (2010) 52001.
[11] J. Casal, M. Rodríguez-Gallardo, J.M. Arias, Phys. Rev. C 88 (2013) 014327.
[12] V. Efimov, Phys. Lett. B 33 (1970) 563.
[13] T. Kraemer, et al., Nature 440 (2006) 315.
[14] P.N. de Faria, et al., Phys. Rev. C 82 (2010) 034602.
[15] A.M. Sánchez-Benítez, et al., Nucl. Phys. A 803 (2008) 30.
[16] M.S. Hussein, R. Lichtenthäler, F.M. Nunes, I.J. Thompson, Phys. Lett. B 91 (2006) 640.
[17] U. Arlt, R. Bass, V. Hartmann, R. Renfordt, K. Sapotta, P. Fröbrich, W. Schäfer, Phys. Rev. C 22 (1980) 1790.
[18] R. Lichtenthäler, et al., Eur. Phys. J. A 25 (2005) 733.
[19] R. Lichtenthäler, et al., Nucl. Phys. News 15 (2005) 25.
[20] T. Matsumoto, et al., Phys. Rev. C 73 (2006) 051602(R).
[21] R. Crespo, E. Cravo, A. Deltuva, M. Rodríguez-Gallardo, A.C. Fonseca, Phys. Rev. C 76 (2007) 014620.
[22] M. Rodríguez-Gallardo, J.M. Arias, J. Gómez-Camacho, R.C. Johnson, A.M. Moro, I.J. Thompson, J.A. Tostevin, Phys. Rev. C 77 (2008) 064609.
[23] D. Baye, P. Capel, P. Descouvemont, Y. Suzuki, Phys. Rev. C 79 (2009) 024607.
[24] M. Rodríguez-Gallardo, J.M. Arias, J. Gómez-Camacho, A.M. Moro, I.J. Thompson, J.A. Tostevin, Phys. Rev. C 80 (2009) 051601(R).
[25] J.A. Lay, A.M. Moro, J.M. Arias, J. Gómez-Camacho, Phys. Rev. C 85 (2012) 054618.
[26] E.C. Pinilla, P. Descouvemont, D. Baye, Phys. Rev. C 85 (2012) 054610.
[27] N. Austern, M. Yahiro, M. Kawai, Phys. Rev. Lett. 63 (1989) 2649.
[28] A.M. Moro, K. Rusek, J.M. Arias, J. Gómez-Camacho, M. Rodríguez-Gallardo, Phys. Rev. C 75 (2007) 064607.
[29] C.M. Perey, F.G. Perey, At. Data Nucl. Data Tables 17 (1976) 1.
[30] B.A. Watson, P. Singh, R. Segel, Phys. Rev. 182 (1969) 977.
[31] M. Avrigeanu, et al., At. Data Nucl. Data Tables 95 (2009) 501.
[32] I.J. Thompson, et al., Nucl. Phys. A 505 (1989) 84.

[33] P. Mohr, et al., Phys. Rev. C 82 (2010) 044606.
[34] P. Mohr, et al., Phys. Rev. C 71 (2005) 017601.
[35] P.R.S. Gomes, et al., Phys. Rev. C 71 (2005) 017601.
[36] P.R.S. Gomes, et al., Phys. Rev. C 71 (2005) 034608.
[37] C. Beck, N. Keeley, A. Diaz-Torres, Phys. Rev. C 75 (2007) 054605.
[38] K.C.C. Pires, et al., private communication.
[39] A. di Pietro, et al., Phys. Rev. C 69 (2004) 044613.
[40] A.M. Sánchez-Benitez, et al., Nucl. Phys. A 803 (2008) 30.